

## THE DIAGNOSTIC POWER OF X-RAY EMISSION LINES IN GRBS

M. BÖTTCHER

*Department of Physics and Astronomy  
Ohio University*

*Athens, OH 45701, USA  
E-mail: mboett@helios.phy.ohio.edu*

Absorption and reprocessing of Gamma-ray burst radiation in the environment of cosmological GRBs can be used as a powerful probe of the elusive nature of their progenitors. Although it is widely accepted that long-duration GRBs are associated with the deaths of massive stars, at least two fundamentally different scenarios concerning the final collapse are currently being considered. Delayed reddened excesses in the optical afterglows of several GRBs indicate that a supernova, possibly of Type Ic, takes place within a few days of a GRB. This supports the collapsar model, where the core of a massive star collapses promptly to a black hole. Variable X-ray features observed in the prompt and afterglow spectra of several GRBs, suggest that a highly metal enriched and dense shell of material surrounds the sources of GRBs. In some cases, evidence for expansion of these shells with velocities of a substantial fraction of the speed of light has been claimed. These observations have been interpreted as support for the supranova model, where a massive star collapses first to a supramassive neutron star, which later collapses to a black hole following loss of rotational support. In this review paper, I will present a brief overview of the current status of the observational evidence for X-ray spectral features in GRBs, and discuss their implications for both the collapsar and the supranova model.

### 1. Introduction: Summary of observed X-ray spectral features in GRBs

The precise localization of gamma-ray bursts (GRBs) by the BeppoSAX satellite, launched in 1996, has facilitated the subsequent discovery of X-ray and optical GRB afterglows, the measurement of redshifts of GRBs and the firm establishment of their cosmological distance scale (at least for long GRBs with durations  $t_{90} \gtrsim 2$  s) beyond any reasonable doubt. The physics of the generally smoothly decaying radio through X-ray continuum afterglow emission is now believed to be rather well understood in terms of the external synchrotron shock model (for recent reviews see, e.g., ref. 29 or 12.) However, in spite of these significant advances, the ultimate source of GRBs is still a matter of vital debate. This is mainly due to the fact that the continuum GRB afterglows are the “smoking gun” of the GRB explosion, revealing only very little information about the initial energy source.

However, even without a direct observation of the central engines of GRBs, it might be possible to infer their nature indirectly if detailed probes of the structure

and composition of their immediate vicinity can be found. A promising candidate for such a probe is high-quality, time resolved X-ray spectroscopy of GRB afterglows. Several high-quality spectra of GRB X-ray afterglows have been obtained from recent observations by *Chandra* and *XMM-Newton*<sup>35,37,46,47,38,10,48,11</sup>. The Swift mission, scheduled for launch early 2004, is expected to give another boost to the study of early X-ray afterglows of GRBs. Previous and currently operating X-ray telescopes have so far (status: December 2003) revealed marginal evidence for X-ray emission lines (mostly consistent with Fe K $\alpha$  fluorescence lines) or radiative recombination edges in 7 GRBs, and one case of a transient X-ray absorption feature at an energy consistent with an iron K absorption edge.

In the following, I will give a brief review of the observed X-ray spectral features in GRBs, before turning to the implications of those observations in general terms. This will be followed by a summary of the currently discussed GRB models which could give rise to the conditions required to produce the observed spectral features.

### 1.1. *X-ray emission lines in GRB afterglows*

Marginal evidence for transient X-ray emission line features in GRB afterglows have been reported for 7 Gamma-ray bursts: GRB 970508<sup>34</sup>, GRB 970828<sup>51</sup>, GRB 991216<sup>35</sup>, GRB 000214<sup>2</sup>, GRB 011211<sup>37</sup>, GRB 020813<sup>11</sup>, and GRB 030227<sup>48</sup>. Tab. 1 lists the key observational features of these seven GRB line detections: (1) the GRB designation, (2) the redshift, (3) the time interval of the line detection, (4) the isotropic luminosity of the emission line, (5) the instrument with which the detection was made, (6) additional remarks concerning the line detection, and (7) the reference to the detection and important contributions through re-analysis of the respective observations. Note that the beginning of the time intervals listed in column (3) are generally set by the beginning of the respective observations, typically several hours –  $\sim 1$  day after the GRB, and might thus not be representative of the onset of the line emission. Only in the case of GRB 030227<sup>48</sup> was a clean, featureless soft X-ray spectrum obtained by *XMM-Newton* in one segment of the observation prior to the segments showing evidence for emission lines. The luminosities quoted in column (4) refer to the Fe K $\alpha$  line emission, unless explicitly noted otherwise.

In the *BeppoSAX* NFI observation of the afterglow of GRB 970508, Piro et al.<sup>34</sup> detected evidence, at the  $\sim 3\sigma$  level, for an emission line feature consistent with a 6.7 keV Fe K $\alpha$  line from highly ionized iron, at the redshift of the burst at  $z = 0.835$ . The X-ray afterglow of this burst exhibited a secondary outburst after  $\sim 6 \times 10^4$  s, and the disappearance of the line from the X-ray spectrum seemed to be coincident with the onset of this secondary X-ray outburst. From a re-analysis of the same observational data, Paerels et al.<sup>32</sup> concluded that a fit using a plasma emission model in photoionization equilibrium, assuming an illuminating continuum identical to the GRB afterglow emission, would either require too large a redshift or too high a temperature for a photoionization-dominated model. This was

Table 1. Summary of the observed X-ray emission lines in GRB afterglows.

GRB	z	$t_{\text{det}}$ [s]	$L_{\text{line}}$ [erg/s]	Instrument	Remarks	References
970508	0.835	$2 \times 10^4 - 5.6 \times 10^4$	$6 \times 10^{44}$	BeppoSAX	second. outburst	34
970828	0.958	$1.2 \times 10^5 - 1.4 \times 10^5$	$5 \times 10^{44}$	ASCA	RRC without line	51, 50
991216	1.00	$1.3 \times 10^5 - 1.5 \times 10^5$	$8 \times 10^{44}$	Chandra ACIS-S + HETG	Broad line + RRC	35
000214	0.47	$4 \times 10^4 - 1.5 \times 10^5$	$4 \times 10^{43}$	BeppoSAX	No OT; z from X-ray line	2
011211	2.14	$4 \times 10^4 - 6.7 \times 10^4$	Si: $6.4 \times 10^{44}$ S: $6.2 \times 10^{44}$	XMM-Newton	No Fe; line det. controversial	37, 10, 38, 39
020813	1.254	$7.6 \times 10^4 - 1.5 \times 10^5$	Si: $1.1 \times 10^{44}$ S: $1.6 \times 10^{44}$	Chandra HETGS	No Fe; low- $\sigma$ Ni	11
030227	$\sim 1.6?$	$7 \times 10^4 - \geq 8 \times 10^4$	Si: $6 \times 10^{44}$ S: $4 \times 10^{44}$	XMM-Newton	No host red shift; no Fe or Ni	48

*Note:* Unless otherwise noted, the luminosity in the 4<sup>th</sup> column refers to the luminosity of the Fe K $\alpha$  line. The start times indicated in the third column generally mark the beginning of the afterglow observation, not the actual onset of the line emission. The remarkable exception is GRB 030227, where the onset of the line emission was directly observed.

interpreted as possible evidence for thermal plasma emission rather than emission from a photoionized plasma.

Interestingly, the second GRB showing evidence for an X-ray emission feature at the redshifted Fe K $\alpha$  energy, GRB 990828, appears to be opposite in that respect. Before the redshift of GRB 970828 could be determined, Yoshida et al.<sup>51</sup> inferred a redshift of  $z = 0.33$  from the energy of the line feature in the *ASCA* spectrum of the afterglow of this GRB, assuming that it corresponds to an Fe K $\alpha$  line at 6.4 keV in the burst rest frame. In a later re-analysis, after the likely host-galaxy identification of GRB 970828, associated with a redshift of  $z = 0.958$ <sup>13</sup>, Yoshida et al.<sup>52</sup> and Yonetoku et al.<sup>50</sup> argued that the emission feature is consistent with this redshift if it is a radiative recombination continuum (RRC) edge rather than a fluorescence or recombination line. They argue that the electron temperature in the plasma responsible for the emission feature is inconsistent with the ionization temperature in thermal equilibrium, and would therefore indicate photoionization as the dominant ionization mechanism.

Marginal evidence for a RRC was also reported for the *Chandra* ACIS-S+HETG spectrum of the afterglow of GRB 991216<sup>35</sup>. Piro et al. (2000) interpret the width and the apparently blue-shifted best-fit energy of the iron line with respect to the redshift of the host galaxy at  $z = 1.00$  as evidence that the Fe line + RRC originate in an outflow with a velocity of  $v \sim 0.1 c$ . If this interpretation is correct, it might be indicative of a supernova explosion a few months prior to the GRB.

For GRB 000214, no optical counterpart could be identified. In this case, the only information concerning its redshift comes from the X-ray emission line detected by the *BeppoSAX* NFI, and was estimated to be  $z = 0.47$ , if the emission line at  $E = (4.7 \pm 0.2)$  keV is interpreted as the redshifted Fe K $\alpha$  line from hydrogen-like iron<sup>2</sup>.

While up to GRB 000214, only evidence for emission features attributable to Fe (or possibly Ni and/or Co) had been detected in GRB afterglows, the observational picture seems to have changed dramatically with more regular GRB afterglow observations by *Chandra* and especially *XMM-Newton*. Reeves et al.<sup>37,38</sup> reported the marginal detection of a set of emission lines in the *XMM-Newton* spectrum of the early afterglow of GRB 011211. If real, these features would be peculiar in that they show evidence for K $\alpha$  lines from the hydrogen-like ions of lighter elements, such as Si XIV, S XVI, Ar XVIII, and Ca XX, but no indication of an Fe K $\alpha$  line or RRC edge. Those lines appear to be blue-shifted by an average of  $v \sim 0.1 c$  with respect to the likely redshift of the burst,  $z = 2.14$ . However, Borozdin & Trudolyubov<sup>10</sup> have pointed out several caveats of the tentative line detections in GRB 011211. (1) The set of low-Z metal emission lines appeared only in the first  $\sim 5$  ksec, prior to a re-pointing of the spacecraft. During that time, the source was located very close to the edge of the CCD chip of the EPIC-pn detector. (2) Evidence for the lines appears only in the EPIC-pn detector, with no such indication in the EPIC-MOS detectors. (3) In their analysis, Borozdin & Trudolyubov<sup>10</sup> find

the *XMM-Newton* spectrum of GRB 011211 consistent with a pure power law, with no evidence for spectral evolution in consecutive time intervals. The addition of an emission line system lowers the reduced  $\chi^2$  from 1.03 to 0.82 (with 8 additional free parameters), which might be an indication of over-fitting, rather than a statistically significant improvement of the fit. A statistical analysis based on a Monte-Carlo simulation approach by Rutledge & Sako<sup>39</sup> yielded a blind-search confidence level of only  $\sim 77 - 82\%$  if the line energies are not restricted to a narrow range around the host-galaxy redshift of  $z = 2.14$ . However, this may have been the result of a coarser energy binning than used by Reeves et al.<sup>37,38</sup>, through which much of the line structure may have been lost. Reeves et al.<sup>38</sup> provided a detailed response to the concerns mentioned above, finding that the results of their initial analysis are robust, but the reliability of the line detection remains controversial to date.

A second example of a set of low-Z element K $\alpha$  emission lines was found in the early afterglow of GRB 020813<sup>11</sup>. The most prominent lines were identified with K $\alpha$  fluorescence line emission from Si XIV and S XVI, blueshifted by  $v = 0.12$  c with respect to the host galaxy red shift of  $z = 1.255$ <sup>4</sup>. The significance of these line detections is quoted at  $\gtrsim 2.9\sigma$ . No Fe line was detected, but weak evidence for Ni emission was found.

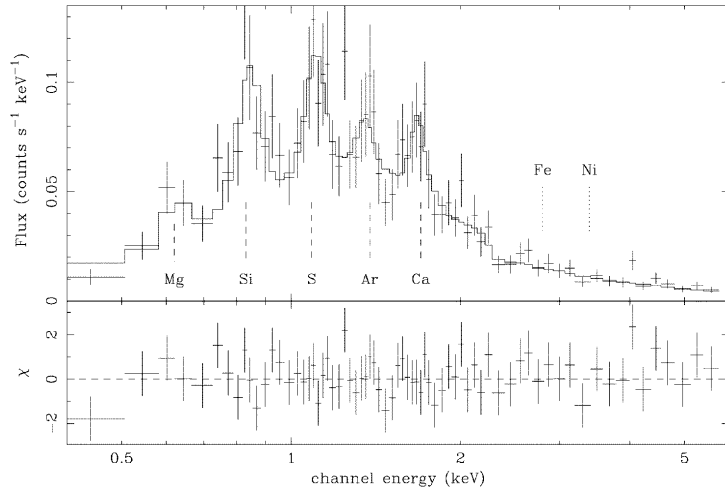


Figure 1. EPIC-pn spectrum of the last 11 ks of the *XMM-Newton* observation of the afterglow of GRB 030227; from Watson et al.<sup>48</sup>

The most recent case (at the time of writing: mid-Dec. 2003) of an emission line detection in a GRB afterglow, namely in GRB 030227<sup>48</sup>, is remarkable in at least two aspects. First, it provided the highest level of confidence of an X-ray line detection to date. Second, it was the first time that the actual onset of the line emission could be determined. As in the case of GRB 011211 and GRB 020813,

emission lines could be attributed only to low-Z elements, specifically, Mg, Si, S, Ar, and Ca (see Fig. 1). The most significant detections were reported from Si XIV and S XVI at red shifts of  $z = 1.32$ , and  $z = 1.34$ , respectively. To date, no independent measurement of the host galaxy red shift has been reported. If the lines are identified with Si and S recombination line emission from material flowing out at  $v \sim 0.1 c$ , as indicated in other cases, then a source red shift of  $z \sim 1.6$  could be inferred. No lines from iron-group elements were detected. GRB 030227 was the first case of a GRB detected by the burst alert system on board *INTEGRAL* to be localized to within a few arc seconds. Note that Mereghetti et al.<sup>28</sup> had previously analyzed the time-averaged *XMM-Newton* spectrum of this observation, in combination with simultaneous *INTEGRAL* observations, and found marginal ( $\sim 3.2\sigma$ ) evidence for an X-ray line at 1.67 keV, which would be coincident with the Ca XX K $\alpha$  line identified by Watson et al.<sup>48</sup>.

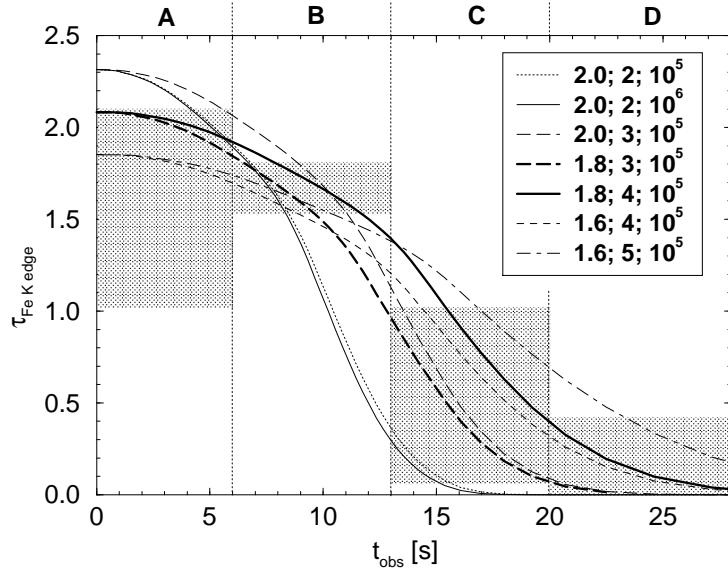


Figure 2. Time evolution of the depth of the transient absorption edge in GRB 990705<sup>1</sup>. The curves indicate fits with a time-dependent photoelectric absorption and photoionization model in a homogeneous shell. The curves are labelled by (column density of material in the shell,  $N_H$  [ $10^{22} \text{ cm}^{-2}$ ], assuming 75-fold overabundance of iron; inner radius of the absorbing shell  $r_{\text{in}}$  [ $10^{18} \text{ cm}$ ]; total density of material in the shell,  $n$  [ $\text{cm}^{-3}$ ]).

### 1.2. The Transient Absorption Feature in GRB 990705

Atomic X-ray absorption features in GRB afterglows are rather common. However, in order to distinguish such features from foreground absorption and to associate them physically with the GRB, one needs to find evidence for variability of those

absorption features on the GRB / early afterglow time scale<sup>33,5</sup>. Until now, only one such case has been observed: In the prompt X-ray emission of GRB 990705, a transient absorption feature has been found at  $(3.8 \pm 0.3)$  keV<sup>1</sup>, consistent with an Fe K absorption edge from neutral iron at  $z = 0.86 \pm 0.17$  at the redshift of the host galaxy at  $z = 0.84$ <sup>21</sup>. This absorption edge was only seen in the first 13 s of the GRB, while no evidence for excess absorption was found in later segments of the *BeppoSAX* WFC observations (see Fig. 2). The best fit to the segment with the most significant detection of the absorption edge (6 – 13 sec.), assuming an underlying power-law absorbed by a neutral absorbing column  $N_H$  with solar abundances and an additional absorption edge yielded a depth of the absorption feature of  $\tau = 1.4 \pm 0.4$  and  $N_H = (3.5 \pm 1.4) \times 10^{22}$  cm<sup>-2</sup>. Leaving the iron abundance in the neutral absorber as a free parameter in a power-law fit to the spectrum in this time segment resulted in  $N_H = (1.32 \pm 0.3) \times 10^{22}$  cm<sup>-2</sup> and a relative overabundance of iron with respect to solar abundances of  $X_{\text{Fe}} = 75 \pm 19$ . Implications and possible interpretations of these results will be discussed in the final section of this review.

## 2. General Constraints

Analytic estimates of the fluorescence and/or recombination line emission in photoionized media in GRB environments have been presented even before their actual detection by several authors (e.g., Refs. 30, 15, 20, 6). A very general estimate of the amount of iron required to produce the observed iron line features can be derived from considering that in the course of complete photoionization of iron, on average  $\sim 5$  Fe K $\alpha$  photons are emitted, since it takes on average  $\sim 12$  X-ray photons to ionize an initially neutral iron atom completely (taking into account the Auger effect), and the K $\alpha$  fluorescence yield is in the range 0.3 – 0.4 for the various ionization stages of iron. In dilute media, if recombination is negligible, it would then take  $N_{\text{Fe}} \sim 2 \times 10^{56} L_{44} t_5$  iron atoms to produce an iron line of isotropic luminosity  $L_{\text{line}} = 10^{44} L_{44}$  ergs s<sup>-1</sup> over a time scale of  $\Delta t = 10^5 t_5$  s. If recombination and multiple ionization of the same iron atom enhance the efficiency of line production, one can introduce an enhancement factor  $f$ , counting the number of times that a single iron atom can effectively contribute 5 K $\alpha$  photons in the process of repeated cycles of ionization and recombination. One then arrives at a general estimate of

$$M_{\text{Fe}} \approx 0.16 \frac{L_{44} t_5}{f} M_{\odot} \quad (1)$$

In dilute, extended media, where recombination is inefficient,  $f \sim 1$ , while in dense media with efficient recombination,  $f \gg 1$ . Due to light travel time effects, the duration of the line emission will be at least  $t_{\text{line}} > R(1+z)(1-\cos\theta_{\text{obs}})/c$ , where  $R$  is the extent of the reprocessing material. Thus, the size limit, together with

the restriction that in the GRBs with line detections, there is no indication for excess X-ray absorption, leads to typical mass estimates of  $M_{\text{Fe}} \sim 0.1 - 1 M_{\odot}$  of iron, confined in  $R \lesssim 10^{-3}$  pc, if the line emission were to originate in a dilute, quasi-isotropic environment. This is unlikely to be realized in any astrophysical setting, and may thus be ruled out<sup>15,5</sup>. Consequently, inhomogeneous media with significant density enhancement outside our line of sight toward the GRB source are required<sup>20,6</sup>.

At this point, several geometries and general scenarios will have to be distinguished. First, the duration  $t_{\text{line}}$  of the line detection can be set either by the light travel time effect, which puts the reprocessor at distances of  $10^{15} \text{ cm} \lesssim R \lesssim 10^{16} \text{ cm}$ . These types of configurations are referred to as *distant reprocessor models*. Alternatively, the duration of the line emission can be determined by the duration of the illumination by a more persistent, gradually decaying central source. In that case, the reprocessor can be located much closer to the source than in the case of the distant reprocessor models. For this reason, these scenarios are referred to as *nearby reprocessor models* (see Fig. 3). Second, we need to distinguish between different mechanisms ionizing the line-emitting iron atoms. The scenarios considered above are generally based on photoionization being the dominant ionization mechanism. However, it is very well conceivable that the material in the vicinity of GRBs is energized by shocks associated with the GRB explosion, and heated to temperatures of  $T \sim 10^7 - 10^8 \text{ K}$  (e.g., Ref. 42). In this case, and for sufficiently high densities, collisional ionization may dominate over photoionization, and the iron K $\alpha$  line emission will be dominated by the recombination lines of H and He-like iron, accompanied by a radiative recombination continuum. We will refer to these models as “thermal models”, as opposed to the “photoionization models” mentioned above.

### 3. Photoionization Models

General parameter studies on photoionization models have been done by many authors. An important complication to keep in mind is the fact that the continuum illuminating the reprocessing material might not be identical or even similar to the observed afterglow emission because, as explained above, the reprocessor has to be located off the line of sight towards the central source of the GRB. As it seems well-established today that GRB emission (at least from long-duration GRBs) is beamed, any emission off the main cone in which a GRB is observed might be different from the actual GRB and afterglow radiation. Furthermore, if the reprocessor is located at a distance of  $R = 10^{15} R_{15} \text{ cm}$ , and illuminated by GRB (and early afterglow) emission from a relativistic blast wave advancing at a coasting speed corresponding to  $\Gamma = 100 \Gamma_2$ , then it will be swept up by the blast wave after a typical illumination time of

$$t_{\text{ill}} \sim 2 \frac{R_{15}}{\Gamma_2^2} \text{ s} \quad (2)$$

unless the blast wave deceleration radius  $r_{\text{dec}} = 5 \times 10^{16} (E_{52}/n_0 \Gamma_2^2)^{1/3}$  cm is much less than  $10^{15}$  cm. Here,  $E_{52}$  is the isotropic equivalent energy of the GRB explosion in units of  $10^{52}$  ergs  $\text{s}^{-1}$  and  $n_0$  is the density of the (homogeneous) surrounding medium in units of  $\text{cm}^{-3}$ . The condition  $r_{\text{dec}} \ll 10^{15}$  cm would require a very low explosion energy directed toward the reprocessor, a large density of the decelerating external medium, and/or a very high bulk Lorentz factor  $\Gamma$ , i. e. a very low baryon contamination.

General studies of the reprocessing efficiency and spectral and temporal signatures of reprocessor models for X-ray emission lines in GRB environments<sup>3,24,16,17</sup> have yielded very useful insight into the general properties of such reprocessing features. The above caveat needs to be taken into account very carefully when applying these results to real GRBs and scaling illuminating spectra, ionization parameters etc., to properties derived from observed continuum afterglows of GRBs.

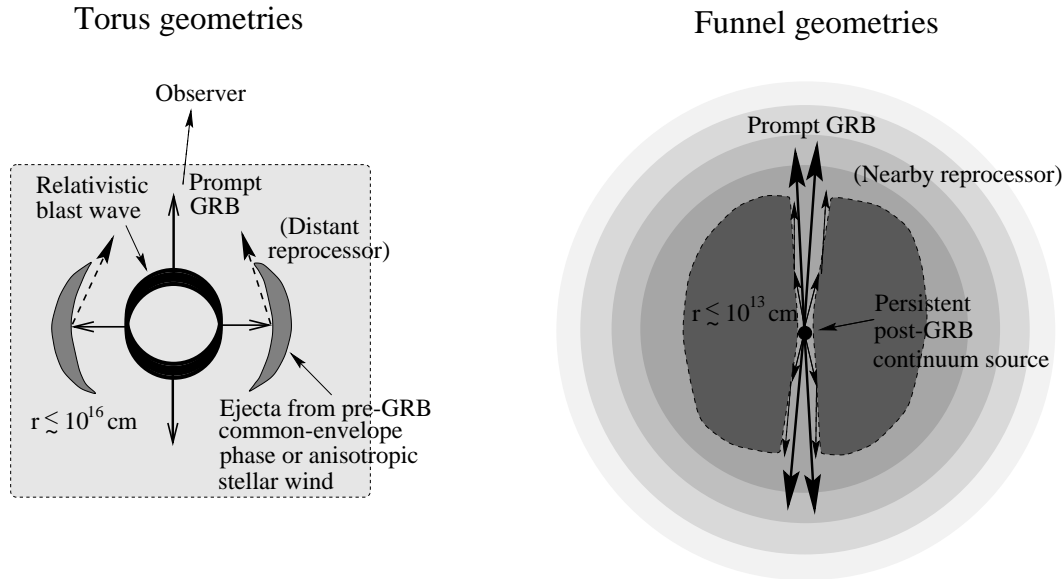


Figure 3. Fundamental geometries of distant reprocessors (left) and nearby reprocessors (right).

In a parameter-independent study in Ref. 24, the efficiency of reprocessing a given ionizing flux into fluorescence and/or recombination line flux has been calculated as a function of ionization parameter. This efficiency is generally at most  $\sim 1\%$  and dependent on the precise spectral shape of the illuminating spectrum. This implies that the observed iron lines listed in Tab. 1 require a total energy in the ionizing continuum of at least  $\sim 10^{51}$  ergs<sup>16</sup>. The reprocessing efficiency is drastically decreasing for high ionization parameters  $\xi \gtrsim 10^3$ . This may provide a diagnostic between distant and nearby reprocessor models<sup>24</sup>.

Another important aspect associated with iron K $\alpha$  line emission is related to radioactive decay of  $^{56}\text{Ni} \rightarrow ^{56}\text{Co} \rightarrow ^{56}\text{Fe}$  in the ejecta of a supernova which may be associated with the GRB<sup>21,26,27</sup>. Since it is primarily  $^{56}\text{Ni}$  that is produced in the final stages of a supernova progenitor, any emission line features should gradually shift in energy from 8 keV for Nickel to 7.4 keV for Cobalt and 6.9 keV for hydrogen-like iron on the radioactive decay time scales of 6.1 d and 78.8 d for  $^{56}\text{Ni}$  and  $^{56}\text{Co}$ , respectively. However, McLaughlin et al.<sup>26</sup> and McLaughlin & Wijers<sup>27</sup> point out the curious detail that  $^{56}\text{Ni}$  would usually predominantly decay via electron capture. Thus, if the reprocessing material happens to be highly ionized, the decay time scale may be significantly longer than in the standard case of neutral  $^{56}\text{Ni}$ . Consequently, for detailed modeling of the “iron” line emission in GRB afterglows, a rest-frame line energy of  $\sim 8$  keV might actually be a more appropriate assumption than the standard value of 6.4 – 6.97 keV. In the remainder of this review, I will, for simplicity, continue to refer to any line feature around  $E \sim 7$  keV in the GRB rest frame as “iron line”, keeping in mind that it might have a significant contribution from Ni and Co.

In addition to light-travel time effects, standard constraints on reprocessor models are obtained considering the ionization and recombination time scales. The ionization time scale may be estimated as

$$t_{\text{ion}} \approx \frac{12}{\int_{E_{\text{thr}}}^{\infty} \Phi_{\text{ion}}(E) \sigma_{\text{pi}}(E) dE} \approx \frac{12(\alpha + 2)}{\sigma_0 \Phi_0 E_{\text{thr}}}, \quad (3)$$

where  $E_{\text{thr}}$  is the photoionization threshold energy,  $\sigma_{\text{pi}}(E) \approx \sigma_0 (E/E_{\text{thr}})^{-3}$  is the photoionization cross section, and  $\Phi(E) = \Phi_0 (E/E_{\text{thr}})^{-\alpha}$  is the ionizing photon flux, assumed to be a straight power-law above the ionization threshold. Appropriate averages for the various ionization stages of iron are  $E_{\text{thr}} \sim 8$  keV and  $\sigma_0 \sim 3.5 \times 10^{20} \text{ cm}^{-2}$ . The recombination time scale can be approximated as

$$t_{\text{rec}} = \frac{1}{n_e \alpha_{\text{rec}}} \approx \frac{10^9 T_4^{3/4}}{n_H (Z_{\text{eff}}/26)^2} \text{ s}, \quad (4)$$

where  $\alpha_{\text{rec}}$  is the recombination coefficient,  $Z_{\text{eff}}$  is the effective nuclear charge,  $T_4$  is the electron temperature in units of  $10^4$  K, and  $n_H$  is the hydrogen number density in units of  $\text{cm}^{-3}$ . The approximation for the recombination rate used above assumes that recombination is dominated by radiative recombination, which becomes inaccurate for ionization states lower than Fe XXV at temperatures above  $\sim 10^5$  K.

Additional model constraints are derived from considerations concerning optical-depth effects due to resonance scattering out of the line of sight (for the resonant Ly $\alpha$  line of Fe XXVI) and Thomson scattering, which define a maximum depth in the reprocessor beyond which the material will effectively no longer contribute to the line emission. Parameter constraints for reprocessor models have recently been summarized in Ref. 40 for the specific purpose of modelling the low-Z element line detections in GRB 011211.

### 3.1. Distant Reprocessor Models

Distant reprocessor models, in which the duration of the line emission is dominated by the light travel time difference,  $t_{\text{line}} \sim R(1+z)(1-\cos\theta_{\text{obs}})/c$ , were the first to be discussed after it became clear that quasi-isotropic fluorescence line emission scenarios were infeasible to explain the observed iron line features<sup>20,6</sup>. Generally, in these models, a photoionizing continuum from the central source, emitted in tandem with the prompt and early afterglow radiation, is impinging on the surface of a strongly anisotropic configuration of dense, pre-ejected material. Recall, however, that the ionizing continuum does by no means have to be identical or even similar to the observed GRB and afterglow emission. The geometry of the reflector is generally taken to be a torus, or a quasi-uniform shell with an evacuated funnel through which the prompt GRB emission can escape unscattered<sup>49</sup>. The pre-ejected tori could plausibly be the result of a common-envelope phase preceding the GRB event. All types of GRB models pertaining to the class of black-hole accretion-disk models, including the collapsar/hypernova and the He-merger (see, e.g., ref. 14 for a review) are likely to have undergone a common-envelope phase prior to the primary's core collapse. The material ejected during such a common-envelope phase is expected to have a directed velocity of the order of the escape velocity from the secondary,  $v \sim \sqrt{2GM_{\text{sec}}/R_{\text{sec}}} \sim 6 \times 10^7 (m/r)^{1/2} \text{ cm s}^{-1}$ , where  $M_{\text{sec}} = m M_{\odot}$  and  $R_{\text{sec}} = r R_{\odot}$  are the secondary's mass and radius. For a detailed discussion of the expected structure of pre-ejected disks / tori, see ref. 8 and references therein. In the collapsar/hypernova models, the delay between the ejection of the primary's hydrogen envelope and the GRB may be as large as 100,000 years, although significant uncertainties about the actual delay time scale remain. Such a long delay would place the pre-ejected material at radii  $R \gg 10^{16} \text{ cm}$ , probably too large to be consistent with the observed time delays of the GRB X-ray emission line features.

Much smaller delays are expected in the He-merger scenario<sup>53</sup> and the supranova model<sup>43</sup>. In the He-merger model, time delays of a few hundred years to a few times 10,000 years may be typical, allowing for both nearby and distant reprocessor scenarios. The supranova model predicts delays of the order of the spin-down time scale of the supramassive neutron star,  $t_{\text{sd}} \sim 10 j_{0.6} \omega_4^{-4} B_{12}^{-2} \text{ yr}$ , where  $j_{0.6}$  is the angular-momentum parameter in units of 0.6,  $\omega_4$  is the angular velocity in units of  $10^4 \text{ s}^{-1}$ , and  $B_{12}$  is the surface magnetic field in units of  $10^{12} \text{ G}$ . Since the typical magnetic field strength is very poorly constrained, delays of several months to several thousands of years might be possible for this model. The ejecta velocity in this case should be more typical of supernova ejecta,  $v \sim 10^9 \text{ cm s}^{-1}$ . Thus it appears that the supranova model may be able to accommodate both distant and nearby reprocessor models as well as the thermal models discussed in the following section.

Different geometrical variations of distant reprocessor models have been discussed in more detail in Refs. 20, 44. Analytical estimates as well as detailed numerical simulations of distant reprocessor scenarios<sup>6,49</sup> indicate a mass requirement

of  $M_{\text{Fe}} \sim 10^{-5} - 10^{-4} M_{\odot}$  for most of the observed Fe K $\alpha$  emission line features observed to date. Note, however, that Vietri et al.<sup>44</sup> derive a significantly higher mass estimate of  $M_{\text{Fe}} \sim 1 M_{\odot}$  for GRB 991216, the most extreme case in terms of total energy emitted in the Fe K $\alpha$  line.

### 3.2. *Nearby Reprocessor Models*

Nearby reprocessors, at typical distances of  $\lesssim 10^{13}$  cm, can either consist of pre-GRB ejecta (see discussion above) or the expanding envelope of a super-giant GRB progenitor<sup>36,26</sup>. In the latter case, if the energy release in the GRB is strongly beamed, the envelope of the progenitor star is expected to remain in a quasi-stable state for a time of the order of the sound-crossing time through the progenitor,  $t_{\text{sc}} \sim 30 m_1^{-1/2} R_{13}^{3/2}$  d, where  $m_1$  is the progenitor mass in units of  $10 M_{\odot}$ , and  $R_{13}$  is its radius in units of  $10^{13}$  cm. It can thus plausibly survive the break-through of an ultrarelativistic jet, and provide a scattering funnel for persistent ionizing radiation throughout the prompt and early afterglow phase of the GRB.

In this class of models, the highly collimated ultrarelativistic outflow most probably associated with the prompt GRB and the continuum afterglow emission, has moved far past the nearby reprocessor at the time the observed emission lines are produced, and can obviously not contribute to the illuminating continuum. Thus, these models require a persistent source of ionizing radiation over at least the duration over which the iron line is observed. Rees & Mészáros<sup>36</sup> suggest that such a source could be provided by the gradually decaying energy flux from a magnetically driven relativistic wind from a fast-rotating, strongly magnetized neutron star (magnetar), if the primary GRB mechanism does not result in the formation of a black hole. They arrive at a required mass of  $M_{\text{Fe}} \sim 10^{-8} M_{\odot}$  of iron in a very thin, ionized skin of the funnel in order to reproduce an iron line with properties as observed in GRB 991216. However, if a similar abundance of iron is distributed throughout the entire stellar envelope, then a mass estimate more in line with the distant reprocessor models ( $M_{\text{Fe}} \sim 10^{-5} - 10^{-4} M_{\odot}$ ) results. These estimates could be reduced if the line emission originates in a dense medium with relativistic electron densities of  $n_{e,\text{rel}} \sim 10^{10} - 10^{11} \text{ cm}^{-3}$ . In such an environment, the line emission could be enhanced by the Čerenkov effect, as pointed out by Wang et al.<sup>45</sup>.

Another variation of nearby reprocessor models has recently been proposed by Kumar & Narayan<sup>19</sup>. They suggest the formation of a scattering screen at a distance of  $\sim 10^{14} - 10^{15}$  cm from the GRB source, possibly as a result of  $\gamma\gamma$  pair creation on back-scattered GRB radiation<sup>41,25</sup>. GRB emission from later (internal) shocks traveling along the jetted ejecta, are scattered back onto the outside of the stellar envelope of the progenitor (the supernova ejecta), and thus provide the ionizing flux for fluorescence line emission (see Fig. 4). This model requires a smaller iron content in the ejecta than previous models since it utilizes a larger fraction of the surface area of the progenitor’s stellar envelope. A possible independent diagnostic of such a model might be delayed high-energy emission due to hadronic

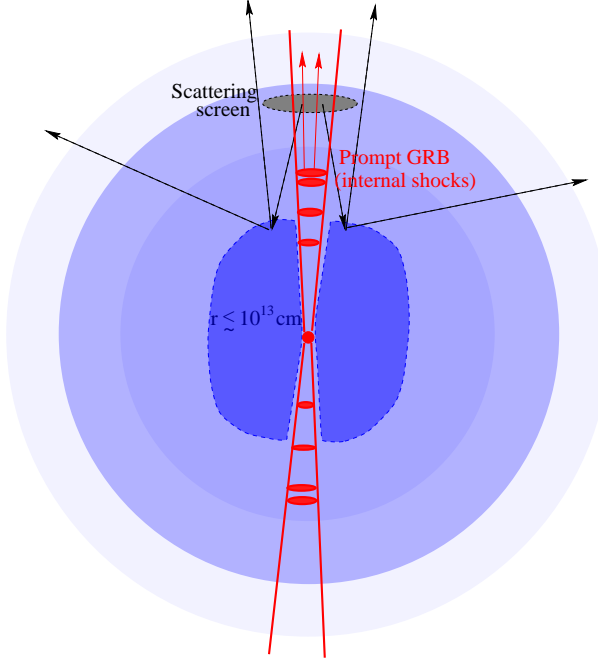


Figure 4. Geometry of the double-scattering model of Refs. 44, 19.

interactions when the GRB blast wave plows into the scattering screen (see, e.g., ref. 18). Kumar & Narayan<sup>19</sup> discuss this model particularly in light of the low-Z emission lines in GRB 011211<sup>37</sup>. In this specific case, their model would require a relatively large pre-GRB outflow rate, producing a density in the surrounding medium of  $n_0 \sim 7 \times 10^7 \text{ cm}^{-3}$ , leading to an external-shock deceleration radius of  $r_{\text{dec}} \lesssim 5 \times 10^{14} \text{ cm}$ . This would correspond to an observed deceleration time scale of  $t_{\text{dec}} \lesssim 0.8 \Gamma_2^{-2} \text{ s}$ , which seems to be in conflict with the duration of  $t_{\text{dur}} \sim 270 \text{ s}$  of GRB 011211, with no indication of rapid variability on the time scale of the order of  $t_{\text{dec}}$ .

#### 4. Thermal Models

As an alternative to photoionization models, Vietri et al.<sup>42</sup> had suggested a thermal model in the framework of the supranova model. They argue that a relativistic fireball associated with the GRB might hit the pre-GRB supernova remnant within  $\sim 10^3 \text{ s}$  and heat the ejecta to  $T \sim 3 \times 10^7 \text{ K}$ . At such temperatures, the plasma emission is expected to show strong thermal bremsstrahlung emission as well as line emission, in particular strong Fe K $\alpha$  recombination line emission. They suggest that the bremsstrahlung and recombination continuum may explain the secondary X-ray outburst observed in GRB 970508. Since the supranova model seems to be

consistent with a large range of SN – GRB delays, one might expect that secondary X-ray outbursts and delayed X-ray emission line features on a variety of time scales can be explained with this type of models. General constraints on thermal emission scenarios for Fe K $\alpha$  lines have also been considered in Ref. 20.

Generic thermal emission models have been applied successfully to the recent observations of lower-Z element emission lines. In all cases, the fits using a collisionally ionized plasma model require a significant over-abundance of low-Z metals compared to solar abundances, with upper limits on the Fe, Ni, and Co abundances lower than the low-Z abundance best-fit values<sup>37,38,11,48</sup>. In the case of GRB 030227<sup>48</sup> (the most significant low-Z element line detection so far), light metal abundances of  $\geq 24$  times solar have been found, while upper limits on the Fe and Ni abundances of 1.6 and 18 times solar abundance were found. Possible implications of these results will be discussed in § 6.

Böttcher & Fryer<sup>8</sup> have investigated the thermal X-ray emission from shock-heated pre-ejected material in alternative progenitor models (i.e. other than the supernova model), such as the collapsar/hypernova and the He-merger model. They found that the He-merger scenario provides a feasible setting for the production of transient Fe K $\alpha$  line emission in the range of luminosities and durations observed. Since both the He-merger and the hypernova/collapsar models are also consistent with much larger SN – GRB delays, they predict that many GRBs may display late-time, thermal X-ray flashes from the shock-heating of pre-ejected material from a common-envelope phase, which could be detected out to redshifts of  $\sim 1$  with currently operating X-ray telescopes.

An alternative scenario based on thermal emission has been suggested by Mészáros & Rees<sup>31</sup>. As the collimated outflow from the central engine of a collapsar is piercing through the stellar envelope of the progenitor, a substantial amount of energy is deposited into the stellar material, which might be highly magnetized. After the jet breaks out of the stellar envelope, this plasma bubble becomes buoyant and emerges through the evacuated funnel of the envelope within  $\sim 10^4 - 10^5$  s. At that time, it may have attained a temperature of  $\sim 10^6 - 10^7$  K, sufficient to produce iron lines, but potentially also a plasma emission spectrum dominated by lower-energy lines, as possibly observed in GRB 011211.

## 5. Implications of the absorption feature in GRB 990705

In principle, inferring constraints on parameters of the circumburster material from observed GRB properties is an easier task than inferring them from emission lines, because in the case of absorption features the continuum responsible for photoionization is identical to the observed GRB and afterglow continuum. Time-dependent X-ray absorption features had been studied for generic, quasi-homogeneous environments in Refs. 5, 15, and for more general cases, including radial gradients, in Refs. 23, 22. For given values of the depth  $\tau_{\text{edge}}$  of an absorption edge and the time scale  $t_{\text{edge}}$  within which it is disappearing, one can directly infer a characteristic radius

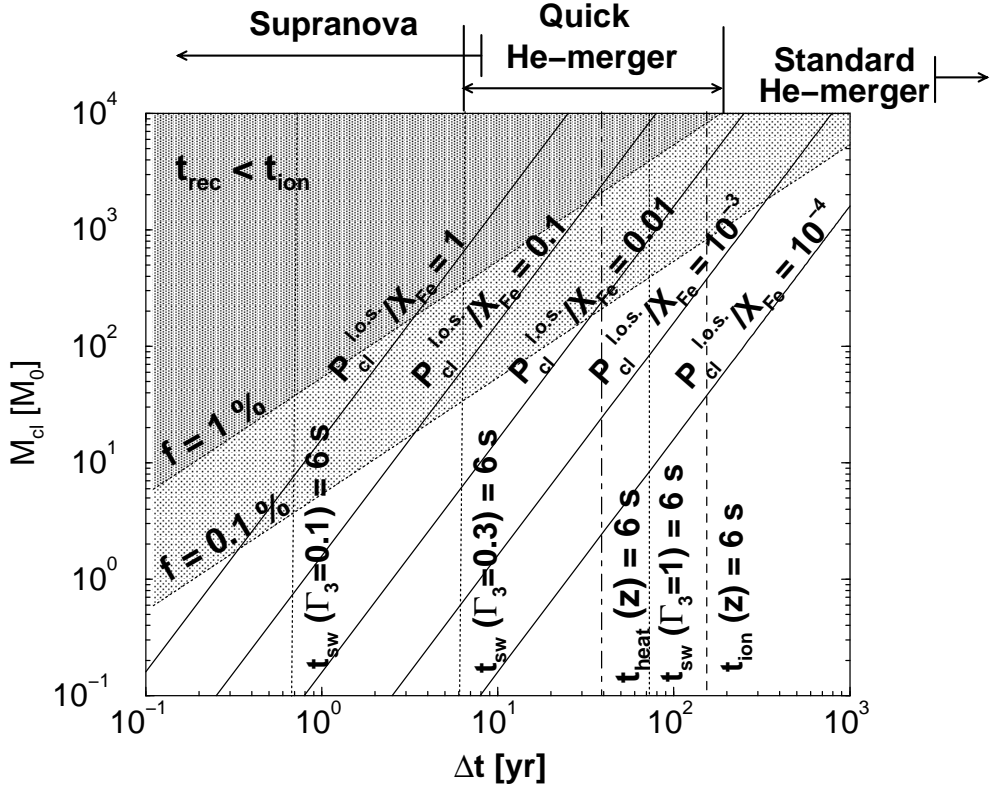


Figure 5. Parameter constraints concerning supernova ejecta mass  $M_{\text{cl}}$  concentrated in dense clumps, and time delay  $\Delta t$  between the primary's supernova explosion and the GRB. Solid lines indicate the condition that an Fe K absorption edge of the depth observed in GRB 990705 is produced for various values of the ratio of the probability  $P_{\text{cl}}^{\text{l.o.s.}}$  of an absorbing cloud being located in the line of sight, to the iron enhancement,  $X_{\text{Fe}}$ , with respect to standard solar system values. Constellations which would give a consistent physical scenario must either be located close to the vertical line corresponding to  $t_{\text{ion}}(z) = 6 \text{ s}$  (if recombination is inefficient) or within the shaded regions in the upper left corner of the plot, which indicates the condition  $t_{\text{rec}} \leq t_{\text{ion}}$  for volume-filling factors of the SN ejecta of 1 % and 0.1 %, respectively, 1 year after the SN.

(by setting  $t_{\text{ion}} = t_{\text{edge}}$ ). Combined with the column density derived from  $\tau_{\text{line}}$ , this allows a direct estimate of the (isotropic) amount of iron in the absorber.

It came as a big surprise that these estimates, applied to the parameters of the transient absorption line in GRB 990705<sup>1</sup>, yielded an estimate of  $M_{\text{Fe}} \sim 44 \Omega M_\odot$  within  $R \lesssim 1.3 \text{ pc}$ , where  $\Omega$  is the solid angle covered by the absorber as seen from the GRB source (see the corresponding fits in Fig. 2). Since this does obviously not seem realistic in any known astrophysical setting, additional effects due to clumping of the absorber in small clouds, in which recombination would become efficient<sup>7</sup>, or resonance scattering of the Fe XXVI Ly $\alpha$  line out of the line of sight<sup>21</sup> had

been considered. Both of these effects could plausibly reduce the necessary amount of iron in the absorber to  $M_{\text{Fe}} \lesssim 1 M_{\odot}$ , but require a rather extreme degree of clumping, with densities of  $n \sim 10^{11} \text{ cm}^{-3}$  in the clumps and distance/size ratios of  $x/r \sim 10^3 - 10^5$ .

Böttcher et al.<sup>9</sup> have scaled the required parameters of the absorber to the clumping properties of supernova ejecta, derived from detailed 3-D hydrodynamics simulations of supernovae. The results were parameterized in terms of the total mass contained in the dense absorbing clouds,  $M_{\text{cl}}$ , and the time delay  $\Delta t$  between the supernova producing the absorbing ejecta, and the GRB. In the case of a supranova scenario,  $\Delta t$  is the delay between the progenitor supernova and the GRB, while in the He-merger scenario,  $\Delta t$  represents the time between the primary's supernova explosion and the He-merger-triggered GRB. Other progenitor models, such as the collapsar/hypernova models, would possess too dilute environments in order to be consistent with the observed properties of GRB 990705. The results of Böttcher et al.<sup>9</sup> are summarized in Fig. 4, and illustrate that all currently discussed GRB models seem to be hard-pressed to produce the required environments to reproduce the transient absorption feature in GRB 990705, with the possible exception of the supranova scenario.

## 6. Summary and Discussion

In this review, I have presented a comprehensive overview of the observed X-ray emission line features in early GRB afterglows and the singular case of a transient X-ray absorption edge during the prompt phase of a GRB. So far, 4 cases of  $\sim 3\sigma$  iron line detections have been found, and 3 cases of lower-energy X-ray emission line features, consistent with  $\text{K}\alpha$  emission from lighter metals without clearly detectable Fe-group emission lines. Models to explain the observed X-ray emission line features can be grouped into photoionization (reflection) and thermal models; reflection models can be further subdivided into distant and nearby reprocessor scenarios.

Generally, the observed  $\text{Fe K}\alpha$  fluorescence or recombination lines could be reasonably well represented by both photoionization and thermal models, though they tend to require rather extreme parameters in terms of iron abundance and total amount of iron in the line-emitting material and/or geometry.

If the observations of  $\text{K}\alpha$  lines of lighter elements without iron-group element fluorescence/recombination lines are real and not related to abundance effects, they might strongly support thermal emission models because any reflection model based on an incident continuum extending into the hard X-ray regime, would naturally also produce strong Fe-group element lines. The suppression of Fe-group lines in reflection models would require a rather unlikely degree of fine-tuning of parameters, e.g., a very soft incident X-ray spectrum and/or an ionization parameter very close to  $\xi \sim 100 \text{ erg cm s}^{-1}$  (see Ref. 24).

One peculiar observation about the presence or absence, respectively of X-ray emission lines in early GRB afterglows seems to be in order here. Tab. 1 shows

that the first 4 cases of line detections (until GRB 000214) all only detected lines consistent with Fe  $K\alpha$  emission; no other lines were found. Intriguingly, the later 3 cases (GRB 011211, GRB 020813, and GRB 030227) all exclusively detected lines of lower-Z elements, but did not find significant evidence for emission lines of iron group elements. This may be in part due to the specific instrument capabilities. *BeppoSAX* had very limited spectral resolution at energies below a few keV and would probably not have been able to detect the low-Z element emission lines found in the later bursts. They were completely outside the sensitive energy range of *ASCA*, and the *Chandra* HETG observation of GRB 991216 was also clearly optimized for line detections around the iron-group element  $K\alpha$  complex. However, the non-detection of any Fe-group line in any GRB afterglow after 000214 — in spite of many rapid follow-up observations by *XMM-Newton* and *Chandra* — may raise some concern about the credibility of the previous detections. An interesting observation in this regard, however, is that all the GRBs with reported Fe-group line detections had hosts at relatively low red shifts of  $z \leq 1$ . In contrast, the later detections of lighter-element  $K\alpha$  emission lines were all associated with GRBs at  $z > 1$  (assuming that the tentative identifications of the lines in GRB 030227 are correct). Also, the low-Z element emission lines in the low-red-shift GRBs all seem to be associated with bulk outflows with velocities  $v \gtrsim 0.1$  c, while the iron-group line detections indicated much smaller outflow velocities, up to  $v \sim 0.05$  c in the case of GRB 991216<sup>35</sup>.

These observations are clearly still based on very-low-number “statistics” and need further confirmation. However, if confirmed, they may reveal information about the cosmological evolution of GRB progenitors. Lower metallicity stars at higher red shifts might suffer less mass loss during their main-sequence life time than stars of the same initial mass during the present cosmological epoch. Consequently, the initial mass threshold for producing a GRB might have been lower in the early Universe than it is at lower red shifts. During a supernova explosion probably associated with a GRB, the outflowing, shocked shells of the progenitor’s envelope would encounter a lower external density, resulting in a higher bulk velocity out to large distances. If the observed bulk velocity is indeed related to the motion of a pre-GRB supernova explosion — as in the supernova model —, this would at least qualitatively explain the observed trends. Extrapolating to very high red shifts, this is consistent with the hypothesis that high-red-shift GRBs may be associated with the almost metal-free (pop. III) earliest populations of stars in the Universe.

## References

1. L. Amati, et al., *Science*, **545**, L39 (2000).
2. L. A. Antonelli, *ApJ*, **545**, L39 (2000).
3. D. R. Ballantyne & E. Ramirez-Ruiz, *ApJ*, **559**, L83 (2001).
4. A. J. Barth, et al., *ApJ*, **584**, L47 (2003).
5. M. Böttcher, et al., *Astron. & Astrophys.*, **343**, 111 (1999).
6. M. Böttcher, *ApJ*, **539**, 102 (2000).

7. M. Böttcher, et al., *AIP Conf. Proc.*, **587**, 190 (2001).
8. M. Böttcher, & C. L. Fryer, *ApJ*, **547**, 338 (2001).
9. M. Böttcher, C. L. Fryer, & C. D. Dermer, *ApJ*, **567**, 441 (2002).
10. K. N. Borozdin, & S. P. Trudolyubov, *ApJ*, **583**, L57 (2003).
11. N. R. Butler, et al., *ApJ*, **597**, 1010 (2003).
12. C. D. Dermer, in *Proc. of XXVII ICRC* (2001).
13. S. G. Djorgowski, et al., *ApJ*, **562**, 654 (2001).
14. C. L. Fryer, S. E. Woosley, & D. H. Hartman, *ApJ*, **526**, 152 (1999).
15. G. Ghisellini, et al., *ApJ*, **517**, 168 (1999).
16. G. Ghisellini, et al., *Astron. & Astrophys.*, **389**, L33 (2002).
17. T. R. Kallman, P. Mészáros, & M. J. Rees, *ApJ*, **593**, 946 (2003).
18. J. I. Katz, *ApJ*, **432**, L27 (1994).
19. P. Kumar, & R. Narayan, *ApJ*, **584**, 895 (2003).
20. D. Lazzati, et al., *MNRAS*, **304**, L31 (1999).
21. D. Lazzati, et al., *ApJ*, **556**, 471 (2001).
22. D. Lazzati, & R. Perna, R., *MNRAS*, **330**, 383 (2002).
23. D. Lazzati, R. Perna, & G. Ghisellini, *MNRAS*, **325**, L19 (2001).
24. D. Lazzati, E. Ramirez-Ruiz, & M. J. Rees, *ApJ*, **572**, L57 (2002).
25. P. Madau, & C. Thompson, *ApJ*, **534**, 239 (2000).
26. G. C. McLaughlin, et al., *ApJ*, **567**, 454 (2002).
27. G. C. McLaughlin, & R. A. M. J. Wijers, *ApJ*, **580**, 1017 (2002).
28. S. Mereghetti, et al., *ApJ*, **590**, L73 (2003).
29. P. Mészáros, *Ann. Rev. of Astron. & Astrophys.*, **40**, 137 (2002).
30. P. Mészáros, & M. J. Rees, *MNRAS*, **299**, L10 (1998).
31. P. Mészáros, & M. J. Rees, *ApJ*, **556**, L37 (2001).
32. F. Paehrels, et al., *ApJ*, **535**, L25 (2000).
33. R. Perna, & A. Loeb, *ApJ*, **501**, 467 (1998).
34. L. Piro, et al., *Astron. & Astrophys. Suppl. Ser.*, **138**, 431 (1999).
35. L. Piro, et al., *Science*, **290**, 955 (2000).
36. M. J. Rees, M. J., & P. Mészáros, P., *ApJ*, **545**, L73 (2000).
37. J. N. Reeves, et al., *Nature*, **416**, 512 (2002).
38. J. N. Reeves, et al., *Astron. & Astrophys.*, **403**, 463 (2003).
39. S. Rutledge, & M. Sako, *MNRAS*, **339**, 600 (2003).
40. F. Tavecchio, G. Ghisellini, & D. Lazzati, *Astron. & Astrophys.*, in press (2003).
41. C. Thompson, & P. Madau, *ApJ*, **538**, 105 (2000).
42. M. Vietri, et al., *MNRAS*, **308**, L29 (1999).
43. M. Vietri, & L. Stella, *ApJ*, **507**, L45 (1998).
44. M. Vietri, et al., *ApJ*, **550**, L43 (2001).
45. W. Wang, Y. Zhao, & J. H. You, *ApJ*, **576**, L37 (2002).
46. D. Watson, et al., *Astron. & Astrophys.*, **393**, L1 (2002a).
47. D. Watson, et al., *Astron. & Astrophys.*, **395**, L41 (2002b).
48. D. Watson, et al., *ApJ*, **595**, L29 (2003).
49. C. Weth, et al., *ApJ*, **534**, 581 (2000).
50. D. Yonetoku, et al., *ApJ*, **557**, L21 (2001).
51. A. Yoshida, et al., *Astron. & Astrophys. Suppl. Ser.*, **138**, 433 (1999).
52. A. Yoshida, et al., *ApJ*, **557**, L27 (2001).
53. W. Zhang, & C. L. Fryer, *ApJ*, **550**, 357 (2001).